Supplementary materials – Hao et al., 2026

Table 1. Primer sequences used for PCR in this study.

Gene	Species	Forward (5′→3′)	Reverse (5′→3′)
Acta2	Mouse	CCCAGACATCAGGGAGTAATGG	TCTATCGGATACTTCAGCGTCA
Col1a1	Mouse	GCTCCTCTTAGGGCCACT	ATTGGGGACCCTTAGGCCAT
Vim	Mouse	TCCACACGCACCTACAGTCT	CCGAGGACCGGGTACATA
Fgf23	Mouse	ATGCTAGGGACCTGCCTTAGA	GGAGCCAAGCAATGGGGAA
Fgfr4	Mouse	CCTTCCACGGGGAGAATCG	CTCCACAAGGCATGTGTATGT
Kl	Mouse	GGGACACTTTCACCCATCACT	ACGTTGTTGTAACTATCGCTGG
Gapdh	Mouse	AGGTCGGTGTGAACGGATTG	GGGGTCGTTGATGGCAACA
Fgfr4	Human	CCATAGGGGACCCCTCGAATAG	CAGCGGAACTTGACGGTGT
PPARG	Human	ACCAAAGTGCAATCAAAGTGA	ATGAGGGAGTTGGAAGGCTCT
GAPDH	Human	ACAACTTTGGTATCGTGGAAGG	GCCATCACGCCACAGTTTCC

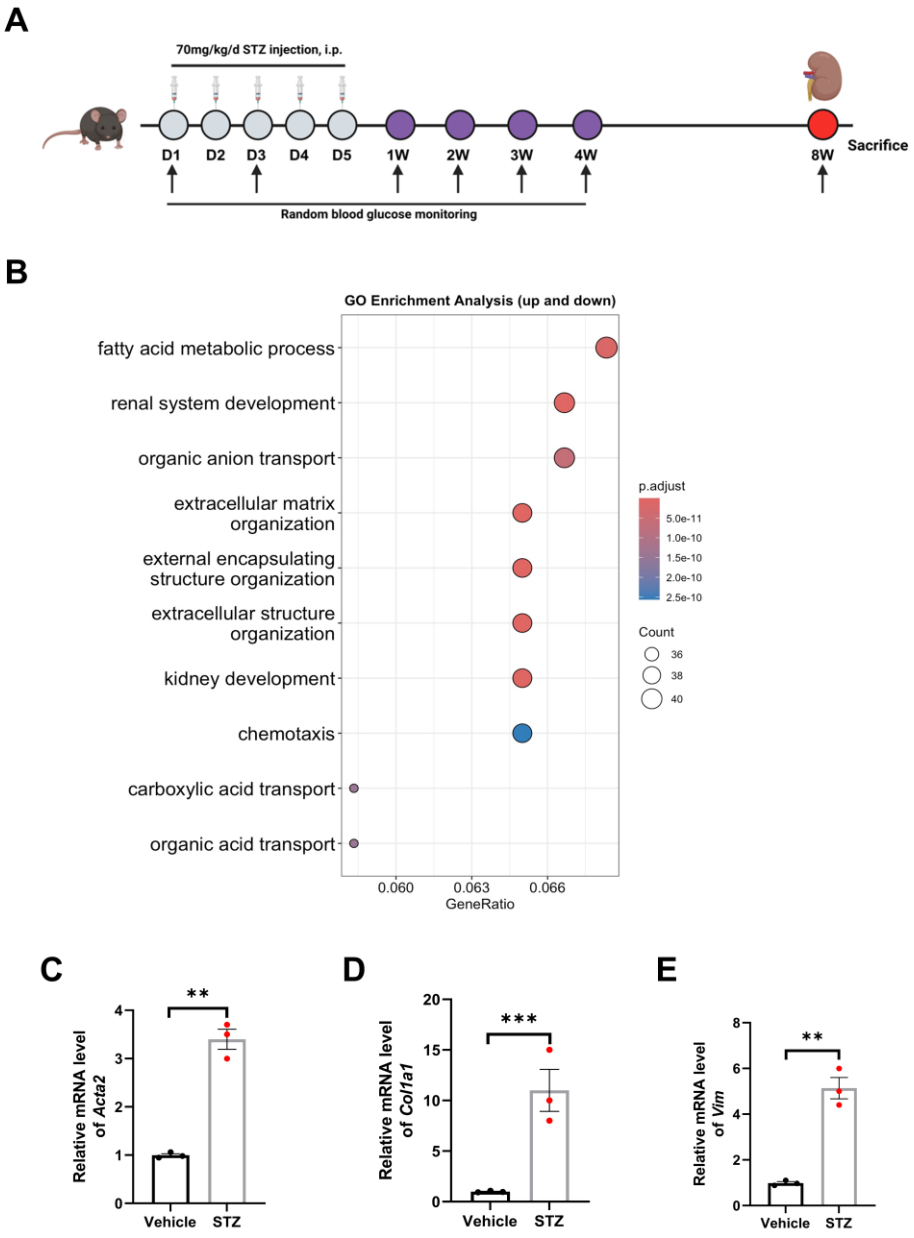

Figure 1. Validation of the STZ-induced diabetic model and GO enrichment analysis. (A) Schematic diagram of the STZ-induced diabetic mouse model during the 8-week experimental period. (B) GO enrichment analysis of differentially expressed genes, showing enrichment of metabolic and fibrosis-related biological processes. (C-E) Relative mRNA expression of *Acta2*, *Col1a1*, and *Vim* in kidney tissues measured by RT-qPCR (n = 3). Data are presented as mean ± SEM. $^{**}p < 0.01$, $^{***}p < 0.001$ versus the control group by unpaired two-tailed Student's t-test.

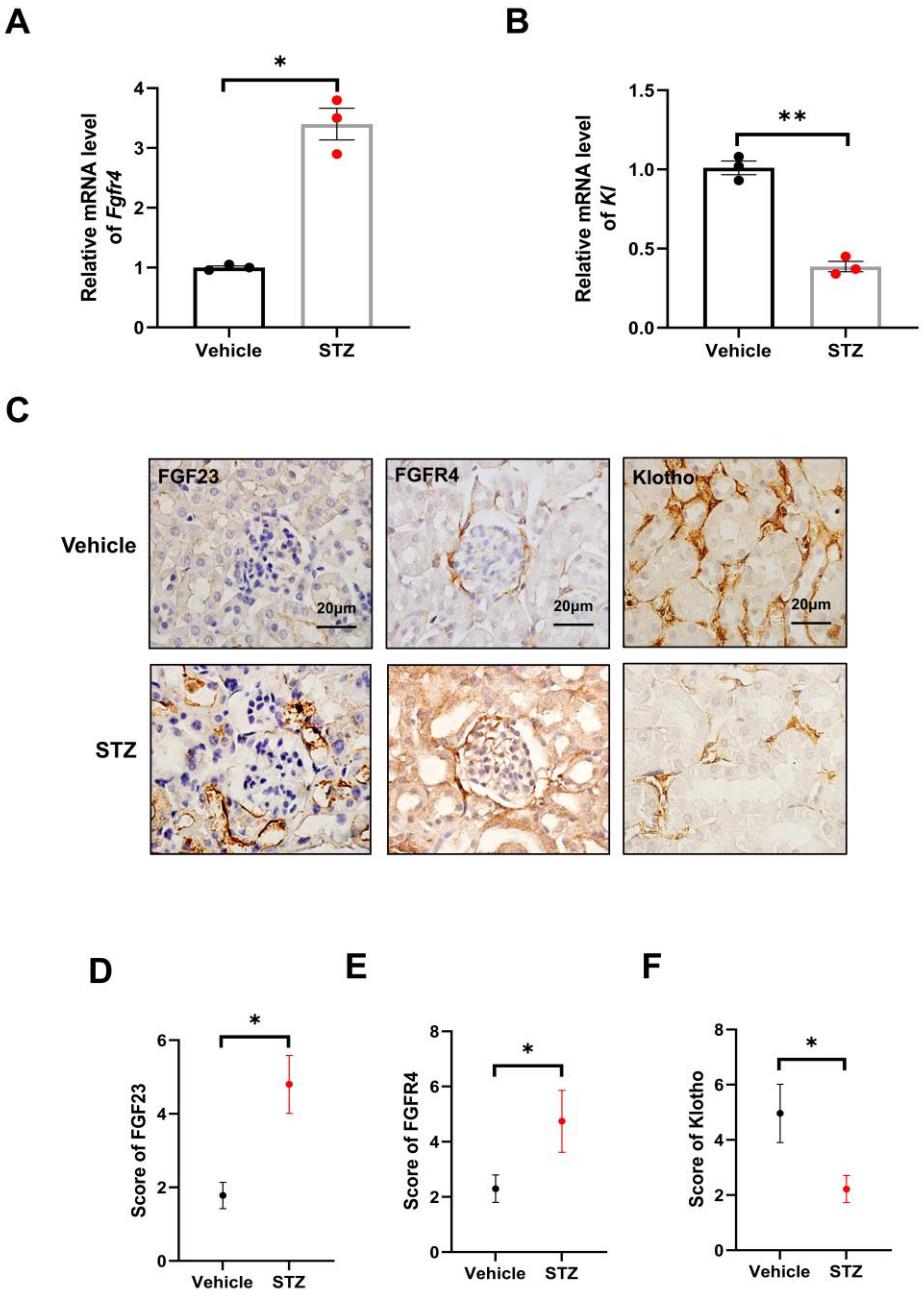

Figure 2. Altered expression of the FGF23-FGFR4-Klotho axis in diabetic kidneys. (A, B) Relative mRNA expression levels of *Fgfr4* and *Kl* (Klotho) in kidney tissues from control and STZ-treated mice. (C) Representative immunohistochemical staining of FGF23, FGFR4, and Klotho in kidney sections. Scale bar: 20 μm. (D-F) Semiquantitative analysis of immunohistochemical staining for the indicated proteins (n = 5). Data are presented as mean ± SEM. *$p < 0.05$, **$p < 0.01$.

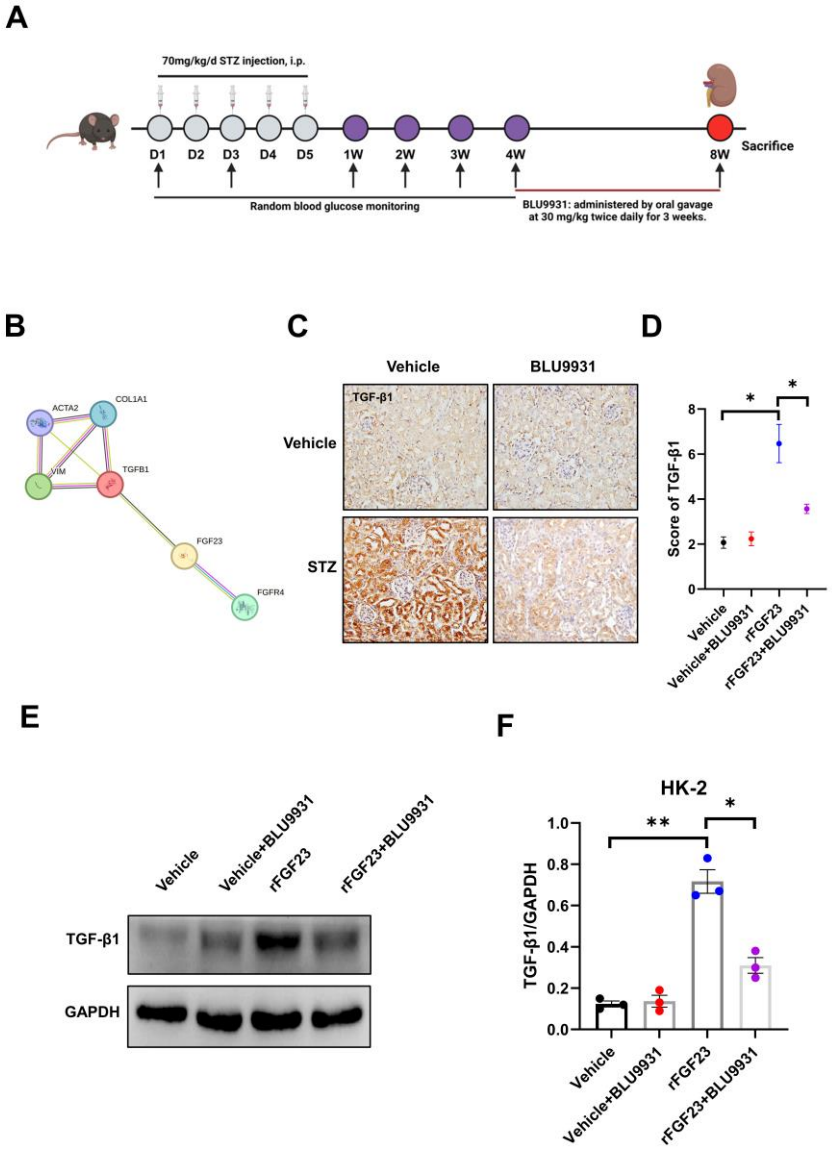

Figure 3. Inhibition of FGFR4 reduced FGF23-induced TGF-β1 expression in vivo and in vitro. (A) Experimental design for treatment with the FGFR4 inhibitor BLU9931. (B) STRING network analysis showing the potential interaction among FGF23, FGFR4, and TGFB1. (C, D) Representative immunohistochemical staining and quantitative analysis of TGF-β1 expression in kidney tissues (n = 5). Scale bar: 50 μm. (E, F) Western blot analysis and densitometric quantification of TGF-β1 protein levels in HK-2 cells treated with rFGF23 in the presence or absence of BLU9931 (n = 3). Protein expression was normalized to GAPDH. Data are presented as mean ± SEM. *$p < 0.05$, **$p < 0.01$.

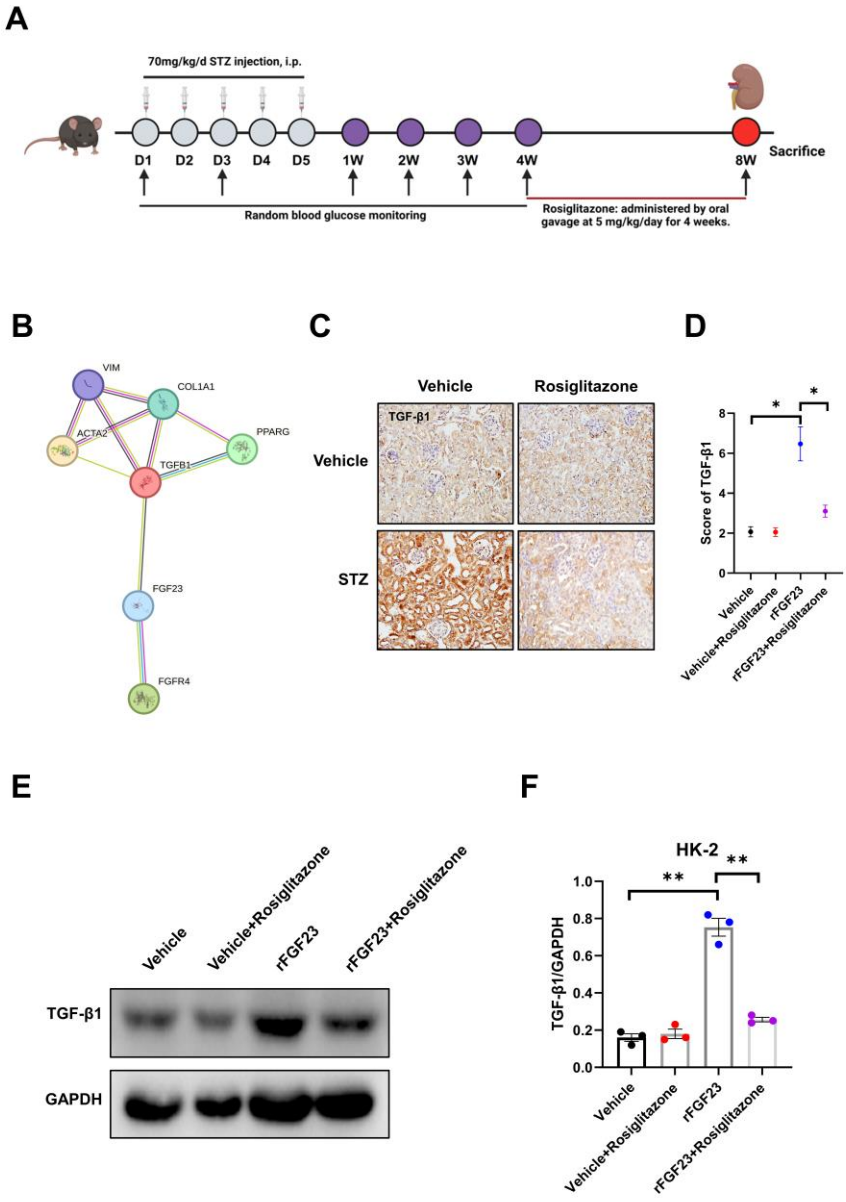

Figure 4. Activation of PPARγ suppressed FGF23-induced TGF-β1 upregulation. (A) Experimental design for rosiglitazone treatment in STZ-induced diabetic mice. (B) STRING network analysis showing the potential association between PPARG and TGFB1. (C, D) Representative immunohistochemical staining and quantitative analysis of TGF-β1 expression in kidney tissues (n = 5). Scale bar: 50 μm. (E, F) Western blot analysis and densitometric quantification of TGF-β1 protein levels in HK-2 cells treated with rFGF23 with or without rosiglitazone (n = 3). Protein expression was normalized to GAPDH. Data are presented as mean ± SEM. *$p < 0.05$, **$p < 0.01$.